Published as: Starink, M.J. (2014) *Thermochimica Acta*, 596, pp. 109-119

A NEW MODEL FOR DIFFUSION-CONTROLLED PRECIPITATION REACTIONS USING THE EXTENDED VOLUME CONCEPT

M.J. Starink

Materials Research Group, Engineering Sciences, University of Southampton, Southampton S017 1BJ, UK

Keywords: kinetic model; diffusion-controlled reactions; nucleation and growth; precipitation kinetics; impingement

Abstract

In this work a new model for diffusion-controlled precipitation reactions is derived, analysed and tested against a wide range of data. The model incorporates elements of the extended volume concept and combines this with a new treatment of soft impingement of diffusion fields. The model derivation involves an integration over iso-concentration regions in the parent phase in the extended volume, which leads to a single analytical equation describing the relation the fraction transformed, α, and the extended volume fraction, α_{ext}, as:

$$\alpha = \{\exp(-2\alpha_{ext})-1\}/(2\alpha_{ext}) + 1$$

The model is compared to a range of new and old data on diffusion-controlled reactions including precipitation reactions and exsolution reactions, showing a very good performance, outperforming classical and recent models. The model allows new interpretation of existing data which, for the first time, show a consistent analysis, in which Avrami constants, n, equal values that are always consistent with transformation theory.

1. Introduction

Diffusion-controlled precipitation reactions are important in a wide variety of commercially important materials. It is important to have available an accurate model for the kinetics of the reaction as heat treatment can determine a range of properties. Preferably such a kinetic model should be accurate, transparent, avoid computationally expensive implementations, and lead to analysis methods that are widely applicable. The objective of this work is to derive and test a new model for diffusion-controlled precipitation reactions that meets these criteria.

Diffusion-controlled precipitation reactions can be thought of as being the combination of 4 overlapping processes: nucleation, growth, soft impingement and coarsening. Several attempts at providing a computationally friendly suitable framework for predicting the progress of diffusion-controlled reactions incorporating a treatment of impingement have been published (see e.g. [1,2,3]), and some less computationally friendly attempts at models have been published more recently [4]. The present paper focuses primarily on the treatment of soft impingement.

One group of existing modelling approaches is based on direct consideration of the diffusion flux at the interface. For instance, the numerical method formulated by Kampmann and Wagner [5], as applied by several authors (e.g. [6,7,8,9]), treats the growth of individual spherical particles following the equation:

$$\frac{dR}{dt} = \frac{\bar{c}(t) - c_m}{c_p - c_m}\frac{D}{R} \qquad (1)$$

where R is the radius of a growing particle, D is the diffusion constant, c_p is the solute concentration in the precipitate, c_m is the solute concentration at the precipitate/matrix interface that is evaluated by the Gibbs-Thompson relationship [10,11], $\bar{c}(t)$ is the mean concentration of the matrix. A characteristic of this approach is that the interaction of the diffusional growth of the various particles is drastically simplified: a spherical geometry of diffusion field is assumed and interaction is described through a single parameter, the mean concentration $\bar{c}(t)$. We can term this a mean field approach.

Some of the users of KW model have described this treatment of impingement as 'a simple response equation' [12], i.e. it is an approximation for which the accuracy is as yet unproven and it has been suggested that the mean field approach underestimates impingement because it ignores a geometrical component to the impingement process [13]. The contribution of a geometrical component has been investigated in [13, 14]. Benefits of the KW approach are that basic capillarity effects can be included and that, in principle and at some computational costs, the numerical scheme can be implemented to model different groups of precipitates and (in principle[1]) incorporate coarsening [7,8]. The models described by Svoboda, Fisher and co-workers [15,16] applying the thermodynamic extremal principle (first described by Onsager [17]) employ a mean field approach that is equivalent to the KW approach (see [16]).

Other works have adopted the extended volume approach (see e.g. [18,19,20,21,22,23]). In this approach the fraction transformed, α, is defined as the ratio of the amount of product phase that has formed and the maximum that can form (on completion of the reaction). Alternatively, we can also define α by the level of depletion of the parent phase (often called the matrix) through

$$\alpha = \frac{\bar{c}(t=0) - \bar{c}(t)}{\bar{c}(t=0) - c_m} \qquad (2)$$

(For discussion on definition of α, see section 4.2.) The extended volume is the imaginary 'volume' in which all growing product phases and diffusion fields expand unimpeded by any of the other product phases and their diffusion fields. In this approach the extended volume fraction, α_{ext}, is defined as the fraction transformed in this imaginary extended volume, and thus $\alpha_{ext}(t)$ increases without limit to infinity. Ignoring various effects including capillarity, α_{ext} is generally given by (e.g.[2,20]):

$$\alpha_{ext} = \frac{(kt)^n}{V_o} \qquad (3)$$

[1] In practice this has proved challenging and generally an additional fittable parameter representing the interfacial energy during the coarsening stage has to be introduced (see e.g. [9]).

where t is the time, k is a factor depending on temperature, composition and (semi-) equilibrium concentrations in the two phases, V_o is the reference volume considered, and n is an exponent (alternately referred to as either the reaction exponent or the 'Avrami exponent'). In the early stage of the reaction impingement is negligible and the constants k and V_o describing this imaginary α_{ext} can always be linked to 'real' progress of the reaction by using $\alpha_{ext} = \alpha$. These models then proceed to derive an equation for the 'real' volume transformed through an analysis that defines the relation between the growth of the extended volume and the real volume transformed. The best known model of this type is the classical Johnson-Mehl-Avrami-Kolmogorov (JMAK) model (after [18,21,24,25]), which is an accurate solution for hard impingement, i.e. where impingement is exclusively due to impingement of growing product phases. Although some authors have used it for diffusion-controlled reactions the JMAK method is not designed for diffusion-controlled reactions, and will in general only be valid in the limited range where no impingement occurs.

The general equation for n is [20,26]:

$$n = N_{\dim} g + B \tag{4}$$

where g is 1 for linear growth or ½ for parabolic (diffusion-controlled) growth, B is 0 in the case of site saturation (no nucleation during the transformation), or 1 for continuous nucleation (at constant nucleation rate), N_{dim} is the dimensionality of the growth. For diffusion-controlled growth n is thus taken as ½, 1 or 1½.

In one extended-volume based model an impingement parameter is introduced, which results in the equation [26,27,28]:

$$\alpha = 1 - \left(\frac{\alpha_{ext}}{\eta_i} + 1 \right)^{-\eta_i} \tag{5}$$

where η_i is the impingement parameter. Through adjusting the impingement parameter this equation can encompass the JMAK model [18,19,21,24,25] (which is obtained for η_i

$\rightarrow \infty$), the lesser known Austin-Rickett [29] equation (which is obtained for η_i=1), and a good approximation for the site saturated case of the KW model is obtained for η_i=5 [2].

Further, several authors [30,31,32] have applied approaches in which impingement of diffusion fields is approximated through approximating diffusion profiles (concentration as a function of the distance to the interface) as linear and subsequently assuming that the progress can be divided into two stages: one where no interaction occurs followed by a stage of interaction.

Phase field methods for simulating precipitation (see eg. [13,33,34]) can reveal many details at the level of single precipitates, but are computationally expensive to the extend that simulation of impingement is rarely attempted (see [13,35] for rare examples of a phase field model with impingement).

As would be expected, all these approaches agree in terms of the prediction of the early stage of transformation in that they all predict the total volume of reaction product to grow according to a power law, Eq. 3. Beyond the initial stage, going into the stage where diffusion fields around particles start to interact, predictions of these models start to increasingly diverge.

The main aim of the present paper is to show that we can derive a computationally efficient kinetic equation that is realistic both in i) the treatment of the distribution of nuclei, i.e. by considering stochastically distributed nuclei, and ii) a diffusion field around each particle with concentration in the parent phase at the interface given by c_m.

2. A new soft impingement model

To derive a new model for diffusion-controlled reactions we start by adopting one of the existing models for nucleation, proceed to calculate the amount the nucleation and initial growth of the phases in the extended volume and, as is done in a range of works [18,26,28], assume that this can be mapped onto Eq. 3, i.e. the parameters of the growth of the extended volume fraction, *k* and *n*, are obtained from the nucleation and initial growth model. Initial growth is here defined as the stage at which α is less than ~0.2, we will show below that during this stage impingement is negligible.

In the present model we will define the extended volume as the imaginary volume in which all diffusion caused by the growth of a single nucleus is unimpeded by the other nuclei. (Note that this is different from some other models, notably [13].) The present model focusses on the diffusion fields in the parent phase, and the fraction transformed is thus obtained from the concentrations in the parent phase, through Eq. 2. The amount of transformed phase (the total volume of the growing nuclei) is directly proportional to this and the absolute values can be obtained from a mass balance equation.

The new element of the model is the treatment of impingement. In the kinetic equation we will characterise the diffusion field as follows. We will define the local depletion fraction of the diffusing species, χ, in the parent phase (the phase in which the diffusion occurs) at position $\bar{x}$ and time t as:

$$\chi(\bar{x},t) = \frac{c(\bar{x},t) - c_m}{c(t=0) - c_m} \qquad (6)$$

where c(t=0) is the starting concentration of the diffusing species in the parent phase. For all locations in the parent phase χ is initially 1 and decreases over time to 0. In the extended volume we can now identify the volumes in which the depletion of the matrix has progressed beyond a certain amount, i.e. we can identify $V(\chi_I)=V_{M2}+V_{M1}(\chi<\chi_I)$ as the volume in which the parent phase M1 with starting concentration c_o has converted to material M2 and depleted M1 with depletion fraction χ_I. We can do this for all values of χ_I and for each we can define a $V(\chi_I)$. We thus have an infinite set of $V(\chi_I)$ in the imaginary extended volume[2], and we need to find a means to approximate the real composition profile in the real volume. We will do that by employing the JMAK impingement theory for each volume and integrate the results for all χ_I.

[2] Thus this imaginary extended volume is a complex concept and the application here differs from that in all other published work known to the author. As an example we could consider nuclei that are spheres. In the extended volume all these spherical nuclei grow preserving their shapes (they remain spheres) and the concentration profile belonging to each nucleus consists of an infinite number of iso-concentration surfaces that are concentric spheres with the nucleus at the centre.

A composition profile in both the imaginary and the real volume is complex and can not be described by simple closed form equations, and as a result the latter integration will not have a closed form solution and will not produce a model that can be captured in closed form solutions. Hence, following the aims of this work, we seek an approximation that both is realistic and *will* produce a closed form solution. To aid to this search for a solution we can consider the JMAK equation as a zero-th order approximation for impingement of diffusion fields[3] in which χ is allowed to be only 0 or 1. In the present new model we take the next order approximation: we take $V(\chi_l)$ to be a linear function. These two cases are illustrated in Fig. 1a and b, here we will consider the case in Fig. 1b.

We can now proceed with the above described integration and we will apply the JMAK impingement theory for each χ_l, i.e. :

$$\alpha = \int_{\chi_l=0}^{\chi_l=1} \left(1-\exp(-p\chi\alpha_{ext})\right) d\chi \tag{7}$$

This integration has an analytical closed-form solution, the solution being:

$$\alpha = \frac{\exp(-2\alpha_{ext})-1}{2\alpha_{ext}} + 1 \tag{8}$$

Here it is used that $V(\chi=0)=0$.

It is noted that as part of this treatment also impingement of interphases (i.e. the surface of the growing nuclei) is accounted for: this is the impingement of the $V(\chi_l=0)$ surfaces.

[3] This approximation is evidently quite poor and the JMAK model was not designed to be used for diffusion controlled reactions. Considering the JMAK model as an approximation for diffusion controlled reactions, as is done here, is intended as a means to introduce the new model and show the relations between the two. It is also worthwhile to reconfirm here that the JMAK model is the correct solution for hard impingement, and stands as a major achievement by early researchers [19,21] in the field. In the present work, comparisons of predictions by the JMAK model on the one hand and mean field models and the new model are merely used to show that, as would be expected, in the impingement stage it produces transformation curves that are vastly different from both the new model and the mean field models.

It is noted that for small α_{ext} the latter equation approximates as:

$$\frac{\exp(-2\alpha_{ext})-1}{2\alpha_{ext}}+1 \cong \alpha_{ext} \quad (9)$$

This confirms mathematically that the initial stage of the transformation is predicted identical to the KW, JMAK, SZ model, and all other models mentioned in the Introduction. This point is further illustrated in Fig. 2 where the model is compared to the JMAK, SZ and KW models. (Here and in subsequent plots of KW model predictions the KW model in the limit for small precipitates is used.) It is seen that in the impingement stage the new model predicts impingement that is very different from the JMAK and KW models. For example, the time from start of a reaction to 90% completion is about twice as long in the new model as compared to the JMAK and KW models. The SZ model prediction is always different from the new model, but comes close to the new model if a specific η_i value of ~2 is chosen. All other models mentioned in the introduction will also provide predictions that are very different from the present new model.

It has been suggested in early work on diffusion-controlled reactions that the solute concentration in the parent phase decreases to its equilibrium following an exponential decay (see e.g. [36]). It can indeed be shown that for α_{ext} increasing, (1-α)/exp(-α_{ext}) approaches asymptotically to a fixed value. Thus, using Eq. 3, also for the present new model for large fractions transformed Eq. 8 approximates to:

$$1-\alpha \cong A\exp(-\frac{t}{\tau}) \quad (10)$$

This is consistent with the analysis of the general shape of transformation curves in the impingement stage provided by Ham [36]. The JMAK and KW models do not possess such an exponential decay and are thus inconsistent with the analysis of impingement in a diffusion-controlled reaction by Ham [36] and by the present work, whilst the model by Fan et al. [32] does possess an exponential decay. (It should be noted that the approach by Ham involves a regular array of particles, which is known [37] to substantially underestimate impingement.)

To further clarify the present treatment a few characteristics are highlighted:

- The model focusses on impingement of iso-concentration profiles in an imaginary extended volume which dominates the approach; impingement of interphases (i.e. the surface of the growing nuclei) is accounted for, but is just a small part of the model.
- Nuclei are distributed stochastically and hence each nucleus has a different environment. Consequently, the new model avoids both the mean field assumption appearing in several models [5,6,8,10,12,15,16] including the KW model [5] and the fixed grain size assumption for growth from grain boundaries [30].
- The new model includes a new treatment of impingement but does not provide a new treatment of nucleation; for nucleation existing treatments will need to be used. Appropriate treatments of nucleation for various reactions can be found in [5,6,30]. The initial growth, before impingement becomes significant, is identical to the KW model [5], and also identical to the JMAK model and models in [4, 20,24,32].
- The model is applicable to 1, 2 and 3 dimensional diffusion-controlled growth of a fixed number of nuclei by using n=½ , 1 and 1½, respectively, and to 1, 2 and 3 dimensional diffusion-controlled growth of nuclei in conditions where the nucleation rate is proportional to 1-α, by using n=1½ , 2 and 2½, respectively.
- Impingement of diffusion fields is treated through an approximation which is thought to be realistic, and avoids simplifying assumptions made in the models highlighted in the introduction.

The model is further schematically illustrated in Fig. 3, which shows a sequence of impingement stages of diffusion fields in one particular geometry: 2 dimensional growth of a fixed number of nuclei (i.e. n=1). In the pictures each grey scale (dark grey to white) represents an interval (a band of values) of the depletion fraction, χ. In this example with 2 dimensional diffusion and all nuclei generated at the same time, iso-depletion contours are segments of circles with constant radius, and a growing nucleus in centre. In 2 dimensional diffusion with continuous nucleation iso-depletion contours are segments of circles with varying radius, and a nucleus in centre. In 3 dimensional diffusion fields depletion contours are segments of spheres.

3. Model assessment and comparison with experimental data

3.1 Scope and overview of model verification

To test the present new model for precipitation kinetics it is applied to data on a range on precipitation reactions. The survey includes all data of isothermal experiments on diffusion-controlled reactions that in the past has been used to support the various kinetic models in [4,23,30,32,38,39] and attempts to avoid any bias other than to exclude the following:

- reactions with product phases of aspect ratio larger than 10 are not yet considered because blocking mechanisms should influence the reaction [26]. (This will be considered in future work [40].)
- data that is incomplete or noisy compared to other data available on the same reaction,
- data for which the identity, distribution or aspect ratio of the phases involved was not reported,
- data on samples for which the distribution of the precipitating elements has been reported to be inhomogeneous prior to the reaction.

A total of over 20 sets of transformation amount vs time data at a wide range of temperatures (310-1770K) were identified, and a summary is presented in Table 1. Microstructural investigations of these materials are provided in the respective papers. For the present work graphs were produced to compare all the experimental data with models, and a summary of comparison with data is provided in Table 1. This Table shows the new model accurately fits the data on all reactions and overall is clearly outperforming all other models. In all cases except one the new model fits with n values limited to be a multiple of ½, as the theory requires. Data on reactions with n=1½ with the most complete datasets[4] are presented in Fig. 4.

[4] All data for which at least 7 datapoints per isothermal transformation/ageing temperature and data for both α<0.05 and α >0.95 is available is presented in this figure. If more than 40 data points are available, averaging over 3 points is employed. For data from [41], one point that is readily identified as outlier is omitted (it deviates more than 20% from the main trend). In all cases of L!$_2$ phase precipitation, reactions in temperature ranges for which two-stage behaviour has been evidenced (see e.g. [41]) are not considered. Data points at times far outside the time range in which the precipitation reaction occurred (by a factor 5 outside the α=<0.01,0.99> range) are not considered.

Alloy / starting material	Precipitate (structure) / reaction	*T* (K)	S	JMAK	KW	GCCB	WLZYZ-FLYZ [32]	Best fitting model / Other model tested	*n*	Experim. data; source and method
Al-0.2% Sc	Al_3Sc (FCC $L1_2$)	603, 543	☑	×	×	-	☑*	New model	2½	[41] fraction transformed by resistivity
Al-0.2% Sc	Al_3Sc (FCC $L1_2$)	503	☑	×	×	-	☑*	New model	1½	[41] fraction transformed by resistivity
Pb–0.08%Ca–2%Sn	$(Pb,Sn)_3Ca$ (FCC $L1_2$)	313	☑	×	x	-	☑*	New model	1½	[43] Fraction transformed by resistivity
Fe-0.37C–1.45Mn–0.11V	allotriomorphic ferrite	973	☑	☑	☑	☑	×**	Several (see text)	½	[30] vol fraction by OM
Fe-0.37C–1.45Mn–0.11V		913	☑	☑	☑	☑		Several (see text)	½	[39] vol fraction by OM
Ni-14 at%Al	Ni_3Al (FCC $L1_2$)	823	☑	×	×	-		New model & phase field simul [35]	1½	[44] size by TEM
$Ti_{0.3}W_{0.4}Cr_{0.3}B_2$	W_2B_5 ($P6_3/mmc$)	1773	☑	×	×	-		New model	2½	[57] by XRD integrated peak intensity
Fe-0.5%C-5%Ni-xSi	bainite	673	☑	×	x	-		New model	1½	[56], vol fraction by dilatometry
Cr-(0.01-0.014)%N	CrN nitride	398-673	☑	×	×	-		New model	1½	[59], vol fraction by resistivity
Fe–0.04 at.% C	austenite (γ) to ferrite (α)	1108	☑	×	×	-		New model	1½	[51] Dilatometry
$Cu_{71.9}Al_{16.6}Mn_{9.3}Ni_2B_{0.2}$	Formation of bainitic plates	473, 503, 523	☑	×	×	-		New model; also SZ with η_i=1 fits	2½	[54] vol fraction by SEM
Al-5.8at%Zn	GP zone (ordered FCC)	403	☑	×	×	-		New model	2½	IC, This work
Clinopyroxene Ca1:99Mg1:64Al0:76Si3:62O12	majoritic garnet M3:15Al1:70Si3:15O12	1723, 1633, 1523	☑	☑	☑	☑		Several	0.4	[63] vol fraction by XRD integrated peak intensity

Table 1: Overview of the diffusion-controlled reactions used in testing the models with best model fitting the data. S= present model (Eq. 8, with Eq. 3), JMAK= Johnson-Mehl-Avrami-Kolmogorov model, KW= Kampman-Wagner model, GCCB= model in [30], WLZYZ-FLYZ= 2 closely related models in [4] and [32].

☑: fits to data within accuracy of experimental data, ×: does not fit data, -: not applicable to reaction. All percentages in wt%, except where noted. IC = isothermal calorimetry, OM = optical microscopy, SEM=scanning electron microscopy, TEM=transmission electron microscopy

* Fan et al. [32] present a model and results which show a good correlation for the data in [41]. It has not been possible to find an independent confirmation of modelling results using this model nor has it been possible to program a working version of this model for the present work.
** Can only fit to data with saturation volume fraction that is inconsistent with data in [48].

This figure shows an excellent correspondence between the new model and all these transformation data sets. In terms of quantity of data used for verification and accuracy of fits, Fig. 4 and Table 1 typically show an improvement by an order of magnitude with existing models referred to here (e.g. [4,24,20,5,5,29,30,32]).

In the below, details on the individual reactions and the data is considered, and further relevant graphs of data are presented. For clarity of figures no error bars are presented, and the reader is referred the original work reporting the data for information on accuracy of data.

3.2 Precipitation of the $L1_2$ Al_3Sc phase in Al-Sc

Røyset and Ryum [41] reported a large set of isothermal transformation data for Al-0.2 wt% Sc alloy samples which were homogenized at 873K for 1h and quenched directly from this temperature to the precipitation temperature. A wide range of temperatures were applied: 463-803K. The isothermally transformed fraction was obtained by observing changes in the electrical conductivity. We will here consider data for transformations in which the microstructural investigations [41] clearly show growth of equiaxed precipitates that are randomly distributed.

The progress of the reaction at 503K and 543K fits excellently to the present model with n=2½, see Fig. 5. The progress of the reaction at 603K fits very well to the present model with n=1½, see Fig. 5. (It is noted that even though the model provides an excellent fit for nearly all data, in some sections the experimental data obtained by Røyset and Ryum [41] in Fig. 5 shows substantial scatter and seemingly inexplicable decreases in fraction transformed. The reasons for this are not known; it is here suggested that

variability in some samples (incl. Sc segregation from casting) and variable quenching conditions could have played a role.)

Røyset and Ryum [41] attempted to fit the JMAK equation to their data. They observed that 'start and end of the transformation the data do not fit very well' [41] and they proceeded to fit the JMAK model to the range of transformed fractions 0.05-0.95, which did fit well provided *n* was taken as about 1.5 to 1.8, and they stated 'this is close to what one would expect in the case where all the precipitates nucleate simultaneously at random sites, but one should keep in mind that the observation of a *n* value in this range is not per se a proof of such a nucleation condition' [41] (see also [42]). The present analysis indicates the data are consistent with the new model, indicates that at 503K and 543K (where *n*=2½) the reaction proceeds with continuous nucleation. Also Fan et al. [32] attempted to fit this data using their model. They obtained a good fit (black lines in Fig. 5), but used a range of fittable parameters. The reader is referred to their publication for their interpretation of this data. It is here noted that for low α, these fits represent $\alpha \sim t^{1.9}$ and $\alpha \sim t^{1.0}$ dependencies which is not consistent with any model for 3D diffusion-controlled growth known to the present author.

3.3 Precipitation of the $L1_2$ $(Pb,Sn)_3Ca$ phase in a Pb–0.08 wt%Ca–2 wt%Sn alloy

Dehmas et al. [43] studied precipitation in Pb–0.08 wt%Ca–x wt%Sn supersaturated alloys (with x = 0.6, 1.2 and 2.0) using TEM observations, hardness measurements and electrical resistivity measurements. The TEM work revealed the formation of spherical $L1_2$ $(Pb,Sn)_3Ca$ phase which were randomly distributed. The kinetics of the reaction were most clearly observed during ageing at 313K, and the data fits excellently to the new model taking *n*=1½. The results are shown in Fig. 4. This analysis further indicates that earlier suggestions based on a JMAK analysis that *n* is about 0.9 which would be due to a complex 2 stage reaction [43], are unreliable.

3.4 Precipitation of the $L1_2$ ordered Ni_3Al precipitates in Ni-Al and Ni-Al-Cr

Data on the evolution of size and volume fraction of $L1_2$ ordered Ni_3Al precipitates in Ni-14 at% Al and Ni–6.5 at%Al–9.5 at%Cr alloys was presented in [44] and [45], respectively, and several interpretations of the data have been published in the literature (see eg. [35,45,46]). In Fig. 7 it is shown that the present model fits the data on evolution of volume fraction and size of $L1_2$ ordered Ni_3Al precipitates in the in Ni–6.5 at%Al–9.5 at%Cr alloy applying diffusion-controlled growth at a constant density of precipitates. In the present model, the evolution of average size of precipitates, d_{av}, in such a reaction can be predicted in a straightforward manner: up to the stage where the density of precipitates starts to decrease due to coarsening d_{av} is proportional to $\alpha^{1/3}$. In Fig. 8 it is shown that the present model fits the data on size evolution of $L1_2$ ordered Ni_3Al precipitates in the in Ni-14 at% Al applying diffusion-controlled growth at a constant density of precipitates (which is consistent with data in [44]), with a limited amount of growth of precipitates prior to reaching the isothermal ageing temperature. Also the data on evolution of size of $L1_2$ ordered Ni_3Al precipitates in the in Ni–6.5 at%Al–9.5 at%Cr alloy fits the present new model. This reveals that the main explanation for this data can be much simpler than hitherto suggested: diffusion-controlled growth at a constant density of precipitates with the novel treatment of impingement describes the data very well up to the stage where coarsening starts to become significant effect (at about t=1000min for Fig. 8).

3.5 Reaction dominated by 1D diffusion: allotriomorphic ferrite formation in micro-alloyed steel

In this work the formation of allotriomorphic ferrite in a Fe-0.37%C-1.45%Mn-0.11%V micro-alloyed steel reported by Garcia and Capdevilla and coworkers [30,39] is also considered, particularly because several authors [4,30,32,39] have used this data to compare against their model, apparently showing a good fit to their models. Ferrite allotriomorphs studied in [30,39] nucleate at the prior austenite grain boundaries and grow both along the boundaries and into the austenite grains. In the experiments described in [30], dilatometric specimens (with different prior austenite grain sizes)

made from 0.37C-1.45Mn-0.11V micro-alloyed steel were first austenitized at 1273 K or at 1523 K for 1 min and then rapidly quenched to 973 K for isothermal annealing for different times. The volume fraction of allotriomorphic ferrite was estimated statistically by a systematic manual point counting procedure [30]. The comparison of this data with various models (Fig. 6) shows that through fitting of the saturation volume fraction all models fit the data with similar accuracy, and also the models described by Garcia and Capdevilla and coworkers [30,39] (which incorporates work by Gilmour et al. [47]), by Fan et al. [32] and by Wang et al. [4] have been shown to fit the data similarly well. (Note that the accuracy of the data point at low *t* may be limited due to the very short times involved; also an incubation time may have occurred.) It is clear that this data can not be used to discern differences in accuracy of the models. (See also Discussion.)

Another point to note here is that calculation of the saturation volume using the austenite solute content at the interface, $C^{\gamma\alpha}$, and the ferrite solute content at the interface, $C^{\alpha\gamma}$, and the gross C content of the alloy, as given by [48] indicates a saturation volume content of about 0.3. This indicates that the models by Fan et al. [32] and Wang et al. [4] are not realistic, as their model fits employ a fitted saturation volume fraction of 0.22.

3.6 Transformation of the austenite (γ) to ferrite (α) and other reactions in steels

Transformation of the austenite (γ) to ferrite (α) phase has attracted the interest of researchers for many decades, and various suggestions for models have been made [49,50,51]. Depending on whether the majority of the free energy is dissipated by the interfacial process or the carbon diffusion, the transformation can be described either as interface controlled or diffusion-controlled in nature [52]. The model by Sietsma and van der Zwaag [50] suggests that for very low C content (<0.1at%) the reaction is diffusion-controlled after a very short interface controlled stage. The literature was searched for isothermal transformation data for this reaction and it was identified that the dilatometry data in [51] obtained during isothermal annealing of an Fe–0.04 at% C alloy at 1108K is the most complete and accurate set of isothermal data, supported by detailed orientation imaging microscopy (OIM) of the resulting microstructures. The

fraction transformed obtained from dilatometry fits was analysed by the new model and was found to fit excellently to the new model (see Fig. 4).

Data on several other reactions in steels have also been assessed. Data on precipitation of σ-phase in base metal, HAZ and weld metal of a 2205 duplex stainless steel weld [53] fits well to the present model (results not presented).

Sutou et al. [54] presented data on volume fraction transformed (formation of bainite plates) vs. ageing time for the transformation in $Cu_{71.9}Al_{16.6}Mn_{9.3}Ni_2B_{0.2}$ shape memory alloys during ageing at 473, 503, 523 and 573K. These curves fit well (within experimental error) to the new model with n=2½ (graphs not presented). This value corresponds with the finding that the density of the bainite plates increased with transformation time. The data set is limited and Sutou et al. showed that with n=2.6 to 2.7 the data also fits well to the SZ model with $\eta_i = 1$ (i.e. the Austin–Rickett equation). If we require that n is a half integer the new model fits best.

Data on the volume fraction of lower bainite formed in high silicon steels precipitated alloys obtained from dilatometry by Chang [55] and by Quidort and Brechet [56] fits well to the present model. (Maximum volume fraction needed to be fitted as no data was presented in the paper.) In this case n=1½.

3.7 Reactions in Cr/Ti and Cr alloys

Data by Bartels et al. [57] on the volume fraction of W_2B_5 precipitated in $Ti_{0.3}W_{0.4}Cr_{0.3}B_2$ alloys fits excellently to the present model. (Maximum volume fraction needed to be fitted as no data was presented in the paper.) In this case n=2½.

Extensive data on precipitation of CrN nitrides [58] in dilute chromium-nitrogen alloys quenched from 1473K and aged between 398K (125°C) and 673K (400°C) has been presented by Weaver [59]. The data fits excellently to the present model with n=1½ (see Fig. 4). At these ageing temperatures, microstructural investigations of these and similar aged alloys shows predominantly equiaxed nitride precipitates which are approximately homogeneously distributed in the Cr rich phase [59,60].

3.8 Reaction with nucleation and 3D growth of equiaxed particles: GP zone formation in Al-Zn

In Fig. 9 data on the fraction transformed vs ageing time at 403K (130°C) for GP zone formation in an Al-5.8 at%Zn alloy is presented. This previously unpublished data was obtained through isothermal ageing of a homogenised and quenched sample in a differential Tian-Calvet microcalorimeter which possesses an excellent base line stability coupled with a high sensitivity (down to a microwatt). The baseline of the apparatus at each temperature was determined by performing experiments with pure Al. Further experimental details are presented in [61,62]. Fig. 9 shows that the new model fits the experimental data very well, whilst other models fail by a large margin. Further checking revealed that all models referred to in this work failed, with the exception of Eq. 5 which, through fitting η_i=2 provides a fit which is even marginally better than the present new model. (But as this involves fitting of an additional parameter, this should not be taken as an indication that Eq. 5 has a distinct advantage.)

4 Discussion

4.1 Comparisons with experimental data and existing models

A summary of comparisons of models with data from the previous section is gathered in Table 1. This Table in conjunction with Fig. 4 to Fig. 9 shows that in nearly all cases the new model is the only fitting model, fitting the data within experimental accuracy. There a few issues on individual reactions that need qualifying.

In the present work also extensive transformation data on a geological material is included through data on exsolution kinetics data of majoritic garnet from clinopyroxene. The present new model provides an excellent fit to the extensive dataset in [63]. The *n* value obtained (*n*=0.4) is close to the *n* value expected for growth from phases nucleated at grain boundaries (*n*=½). This is further supported by SEM studies in [63] which show the majoritic garnet was exsolved along the grain boundaries of parent clinopyroxene. The present finding of the good fit of the new model solves the apparent contradiction that in a range of works on diffusion-controlled reactions in geological

materials / minerals (see e.g. [63,64] and references therein) the kinetic behaviour of has been successfully modelled using the JMAK model. It is thus recommended that in these cases it is checked if the present new model also provides a good or even better fit to the data.

In the case of allotriomorphic ferrite formation, the equilibrium volume fraction cannot be reliably determined which means that several models potentially fit the data. This is related to the fact that reactions with n close to 0.5 stretch over a large range of reaction times: considering that for the present new model $t(\alpha=0.995)/\ t(\alpha=0.005)=2\ 10^4$ data on such reactions needs to stretch over a time range of about 4 decades before it can be reliably used to discern relative accuracy of different models. None of the data sets for reactions with n close to 0.5 that were identified in the present extensive search meets the strict requirement of showing the range $\alpha=<0.005,0.0995>$ or stretching over a time range in excess of 4 decades, and hence it is not possible to discern the relative accuracies of the various models for these types of reactions. It is here suggested that this fundamental issue is one cause of the proliferation of various models: typical datasets on amount of product phase for a reactions with n=0.5 can be made to apparently fit a wide variety of models. So even though data in [30] fits the JMAK model and the models by Garcia de Andres et al. [30] and by Fan et al. [32] quite well, it is not sufficient to support the general validity of the treatment of impingement in these models. It is here suggested that, seen in the light of the other comparisons and theory presented in the present paper, Fig. 6 supports the present new model.

In the one case where a phase field simulation is available, for the precipitate size evolution in a Ni-Al alloy, this is seen to fit the data well, whilst the new model is marginally better. Clearly phase field models offer a strong potential, but this needs to be weighed up against the much more computationally friendly nature of the present model. When rapid assessment of data is needed the present model is clearly a preferred first step, and may well provide a full analysis without the need for further, more computational expensive simulations. (See also Section 4.3.)

A comparison of model predictions by the Fan et al. model [32] is available for a very limited number of reactions, all selected by Fan and co-workers. An extensive search shows that this model has not been applied beyond the group in which it was derived,

whilst for the present work it has not been possible to program a working version of this model. Whilst the model in [32] should provide results that are in many respects comparable to the present model, a few remarks are made.

- The main concept of the present model and the model in [32] has similarities, notably in that both use linear approximations. In the present model $V(\chi_I)$ is approximated using a linear section (see Fig. 1), but this is different from procedure used in [32].
- In the model in [32] (and also [30]) there will be a discontinuity in $d\alpha/dt$ - a 'kink' in the $\alpha(t)$ curve - at what has been termed the "initiating point of soft impingement" [32]. Such a discontinuity has never been evidenced, and extensive experimental work on diffusion controlled reactions using techniques that measure a signal that is proportional to $d\alpha/dt$, such as isothermal and non-isothermal calorimetry in [2, 26,27,28,61,62,65,66], shows no discontinuity. (See Fig. 7 in [39] for an inconclusive attempt to show such a discontinuity.) The present new model has no discontinuity in $d\alpha/dt$; its stochastic nature ensures that soft impingement gradually increases during the reaction from growth that is unimpeded to asymptotic behaviour when impingement is severe. In this sense the new model is akin to other models that employ the extended volume concept [20,23,27,28] and fundamentally different from the models in [30,32,39].
- The model in [32] uses 28 equations, and through employing the present expanded version of an extended volume concept the present model can be explained using just 3 equations Eqs. (3,4,8). There are benefits that derive from this more transparent formulation, see section 4.3.
- A comparison of data on precipitation in an Al-Si alloy [66] with a non-isothermal version of the Fan et al. model [32] in [67] shows that the fit of the Fan et al. model is not as good as the fit to another model reported in [66].

All models considered in the present work [3,4,5,6,7,15,16,23,27,28] including the new model contain assumptions and simplifications. This is necessary caused by the complexity of the diffusion fields. In several models [3,5,6,7,15,16] the mean field assumption is the key simplifying assumption, and the present assessment shows that this results in a poor fit to experimental data. In fact it should be clear that a mean field assumption introduces inaccuracies: in any real diffusion controlled reaction each

growing product phase should have a different environment. Adopting a mean field assumption will produce transformation curves that overestimate the reaction rate in the impingement stage. The new model avoids this apparently unsuitable assumption and instead makes another key simplifying assumption: it assumes that we take V(χ_I) to be a linear function. Also this assumption should at present be treated as a simplifying assumption: although it is likely to provide a good approximation, no theoretical justification is available, and any (small) deviations introduced by this assumption need further theoretical analysis. However, it is clear that the available experimental evidence, as reviewed in Section 3, supports that the new model is highly accurate.

4.2 Definition of the fraction transformed

In the derivations of the present model the fraction transformed, α, was defined as per Eq. 2, i.e. it is based on the depletion of solute in the parent phase. This is key to the model as it allows the present approach based on impinging diffusion fields. This definition of α relates closely to experimental methods of measuring fraction transformed that are based on properties of the parent phase; these methods include electrical conductivity measurements [3,41,43,59], lattice parameter change determination [68,69] and thermoelectric power [70,71,72]. However, another way of defining α is based on the volume fraction, i.e. α is proportional to the amount of product phase. This method is closely related to experimental determinations of fraction transformed based on microscopy and tomography methods. To distinguish the two we will use the symbols α_{pa} and α_{vol}. The difference α_{pa}-α_{vol} can be determined through evaluating the appropriate mass balance equations and this shows that α_{pa}-α_{vol} is close to zero for small volume fraction of product phase and, when averaged during the transformation, this differential increases with volume fraction. It reaches 0.016 for reactions with a maximum volume fraction of 0.1. This means that for nearly all reactions considered here the effect is smaller than any experimental uncertainty; and only for formation of $L1_2$ ordered Ni_3Al precipitates in Ni based alloys will this difference become noticeable.

A possible solution for addressing this deviation that occurs due to α_{pa}-α_{vol} rising for larger volume fractions is to apply a correction using α_{pa}-α_{vol} obtained from the mass balance equation. This will form part of future work [40].

4.3 Further beneficial features of the new model and further work

Models such as the SZ and JMAK models are extensively used to determine the reaction exponent (a.k.a. Avrami exponent) from the slope of a plot of a certain function of $(1-\alpha)^{-1}$ vs ln$t$ [73] (for the JMAK model this is ln ln$((1-\alpha)^{-1})$ vs ln$t$). The present model also allows such an analysis, and thus will provide a valuable analysis tool [40]. This is one of the beneficial features which will be briefly indicated here, to be further developed in future work [40].

The present new model also allows prediction of the size distributions of precipitates, within the concept of continuous nucleation (B=1) and fixed number of nuclei (B=0). It will also be possible to extend the model to highly elongated particles. A full analysis is left to future work [40].

It is also noted that a plot the reaction exponent n as a function of the ratio of the transformation temperature and the maximum temperature of stability of the reaction product shows a perfect two stage behaviour, with n=1½ for a low ratio and n=2½ for ratios above a threshold value. This can be used to analyse the mechanisms of nucleation and saturation of nucleation, which will be reported in future work [40].

5. Conclusions

A new model for diffusion-controlled reactions focussing on the impingement stage has been derived. The model incorporates elements of the extended volume concept and combines this with a new treatment of soft impingement of diffusion fields. The new treatment captures the relation between the (imaginary) extended volume and the actual fraction transformed in a single analytical equation. A consequence of the model is that the impingement stage approximates to an exponential decay of diffusing species, which is consistent with the analysis of the general shape of transformation curves in the impingement stage provided by Ham [36]. The new model is compared to an extensive range of datasets, and a very good correspondence is shown. This level of

experimental verification substantially exceeds that published for other models. The model solves a number of inconsistencies in the literature and should be used as a first recourse to fit and analyse data on diffusion-controlled reactions.

Acknowledgements

Dr A.-M. Zahra is gratefully acknowledged for performing the isothermal microcalorimetry experiments on the Al-Zn alloy.

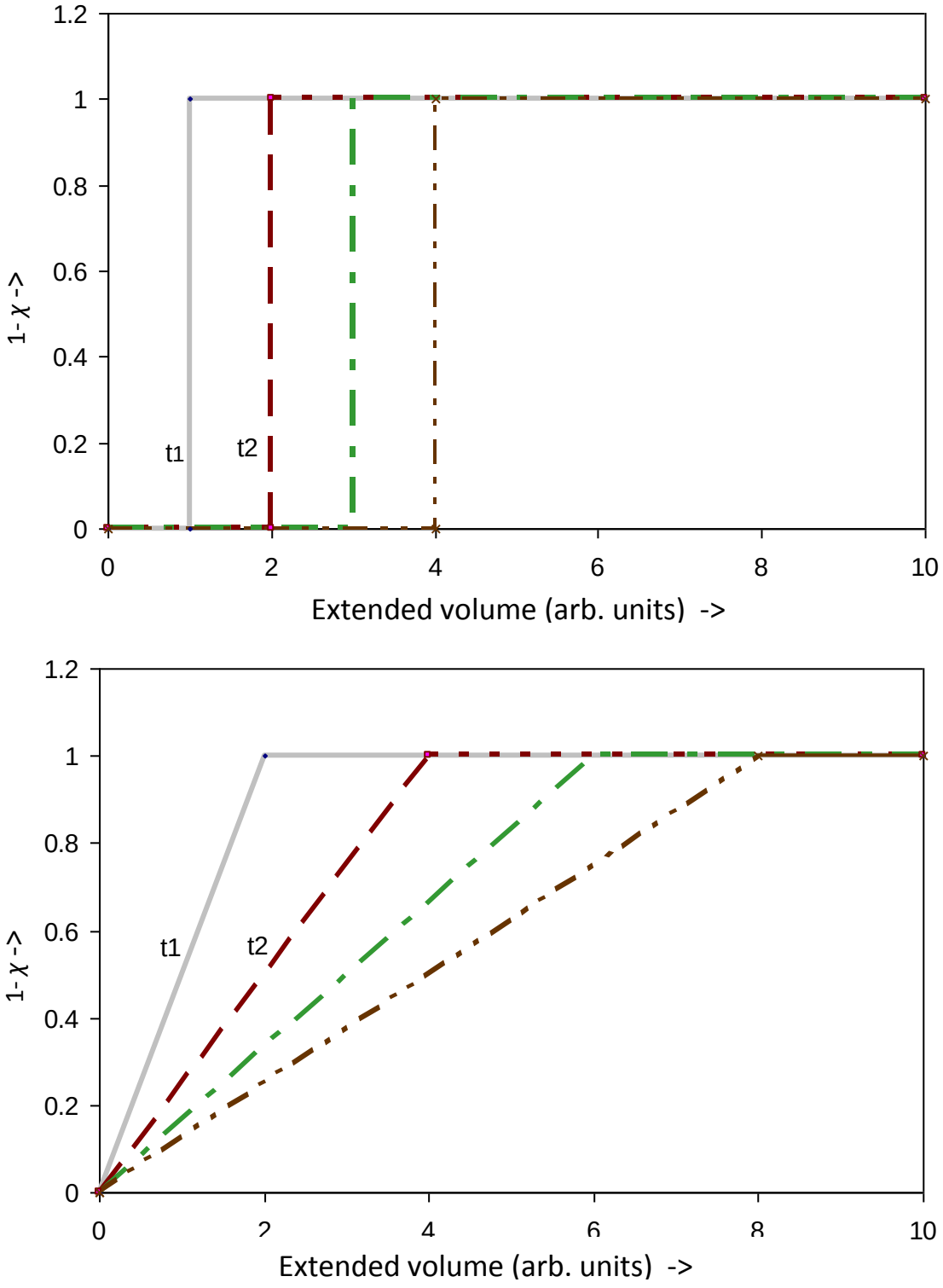

Fig 1. Schematic depiction of the depletion fraction (1- χ) as a function of the volume in the extended volume for a diffusion-controlled reaction a) approximation used if one was to use JMAK kinetics to approximate a diffusion-controlled reaction (a poor approximation), and b) linear $\chi - V$ approximation (the much improved approximation used to derive the present new model).

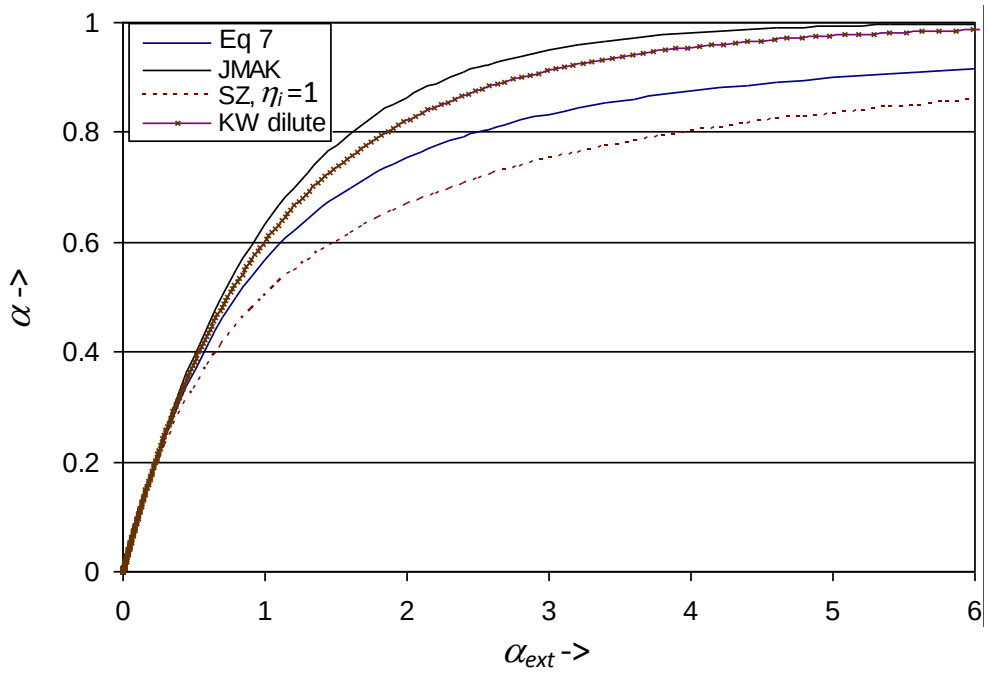

Fig 2. Fraction transformed vs extended fraction transformed for 4 models: Kampmann Wagner (KW) for a dilute alloy, Starink-Zahra (SZ) for η_i=1, JMAK and the present new model (Eq. 7).

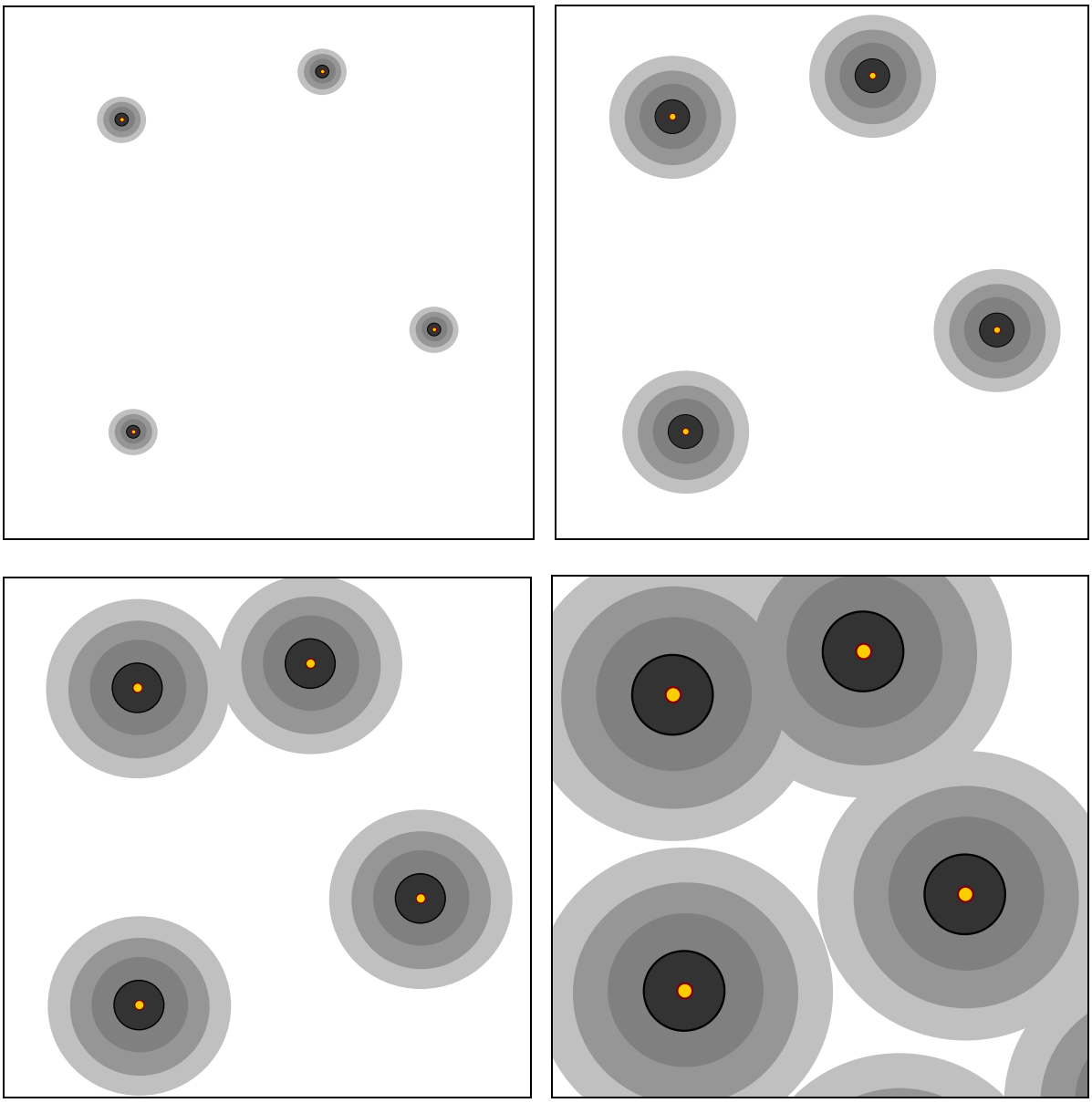

Fig 3. Schematic illustration of impingement for 2 dimensional growth of a fixed number of nuclei. There are 4 nuclei in this section (yellow) with a partially depleted matrix around them. Each grey scale represents an interval of the depletion fraction, χ. Iso depletion contours are segments of circles.

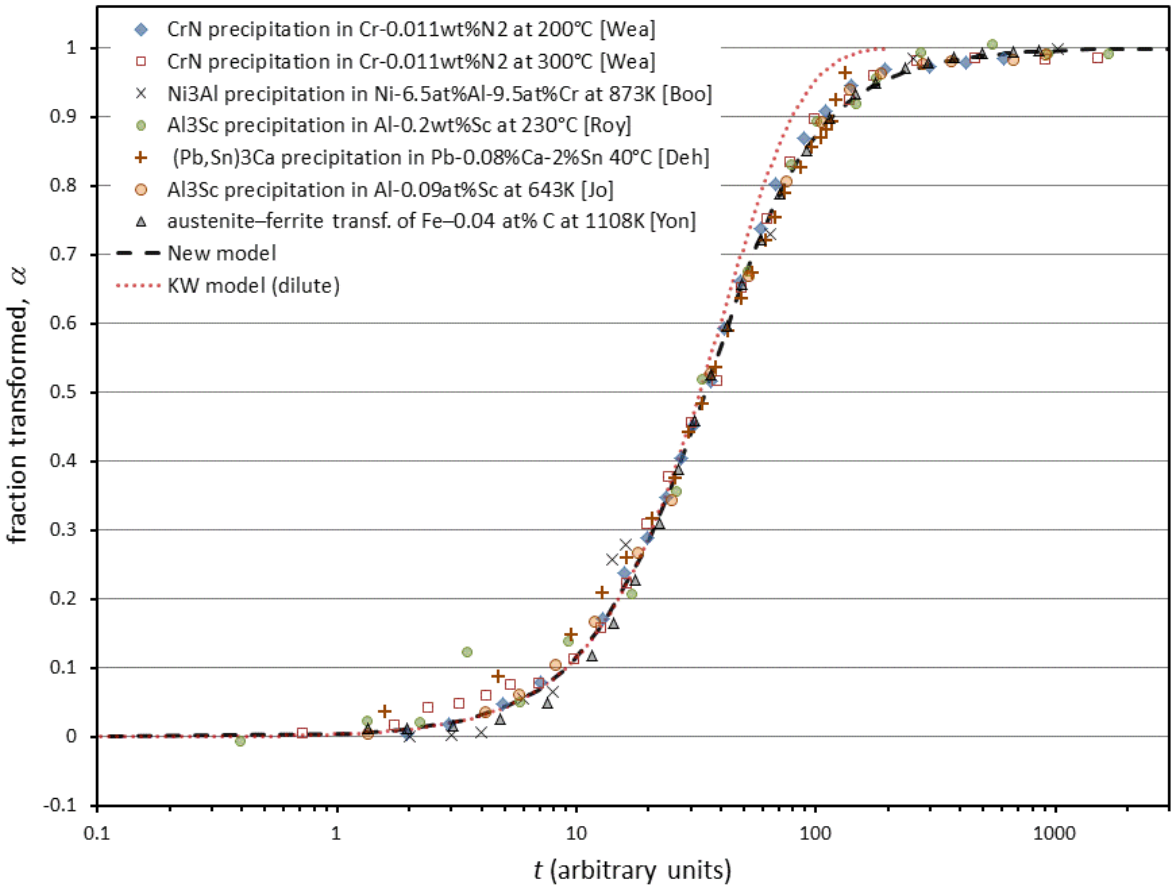

Fig 4. Fraction transformed for various precipitation reactions vs t/A, with t the isothermal ageing time and A for each reaction chosen such that $t(\alpha=0.5)$ coincides. Data from [Wea]=[57], [Boo]=[43], [Roy]=[39], [Deh]=[41], [Jo]=[40], [Yon]=[49].

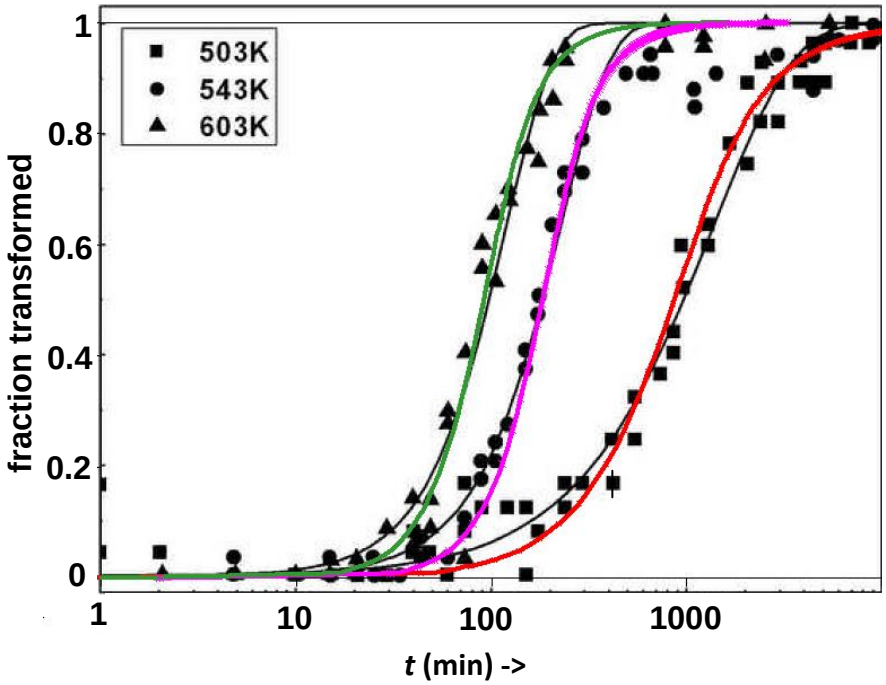

Fig 5. Fraction transformed vs the ageing time, t, for on Al_3Sc formation in Al-0.2 wt% Sc from Røyset and Ryum [39]. Black lines are model calculations reported by Fan et al. [30] using their model [30], colored lines are the present model with n=2½ (for the 2 higher temperatures) and n=1½ for the lower temperature.

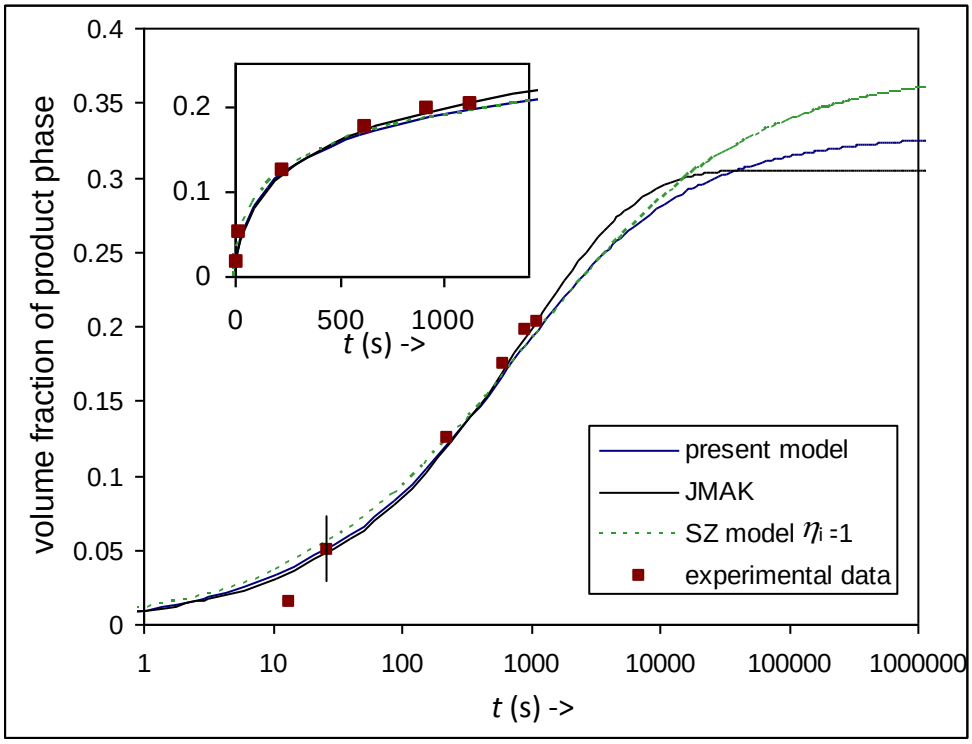

Fig 6. Amount of product phase vs the annealing time, *t*, in ferrite formation in isothermal annealing of 0.37C-1.45Mn-0.11V micro-alloyed steel with prior austenite grain size 76 µm. Specimens was austenitized at 1523 (1273) K for 1 min and then rapidly quenched to 973 K for isothermal annealing. Data from [28]. Experimental data is compared with 4 models with k=0.011, n=0.5. Main graph is on log time scale, inset on linear time scale.

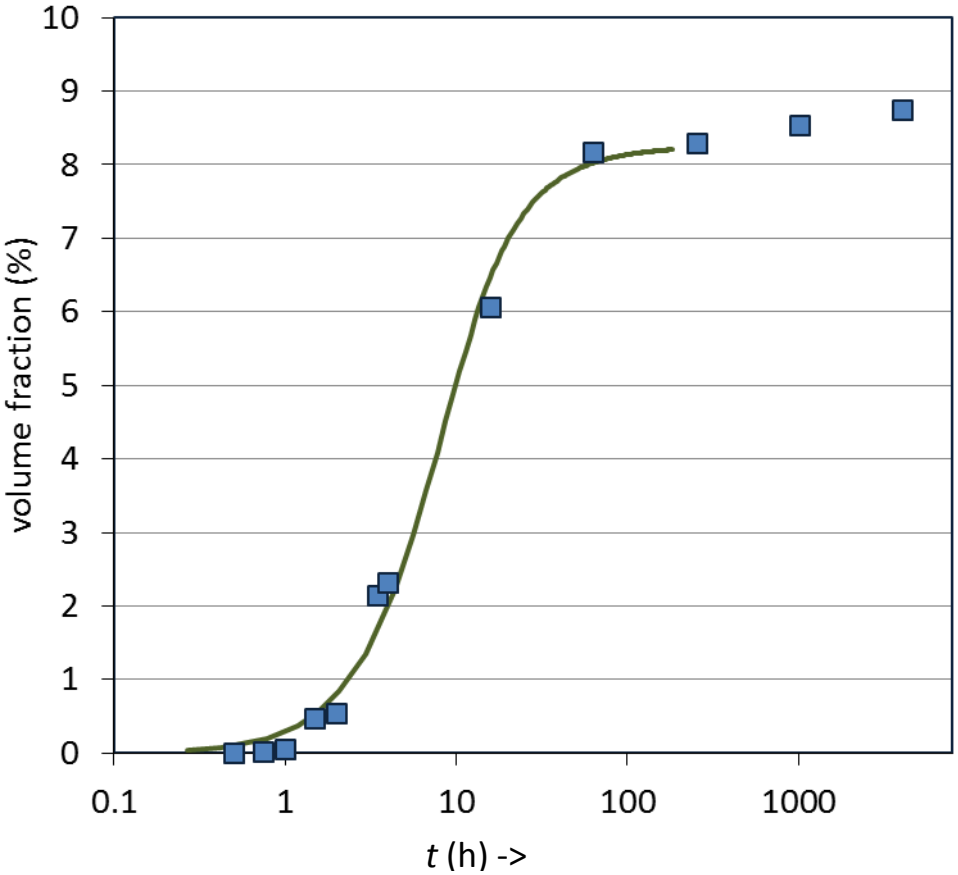
10
9
8
7
6
5
4
3
2
1
0
volume fraction (%)
0.1
1
10
100
1000
t (h) ->
Fig 7. The evolution of the precipitate volume fraction for Ni– 6.5 at% Al–9.5 at% Cr at 873 K (data from Booth-Morrison et al. [43]). The volume fraction in is fitted by the new model.

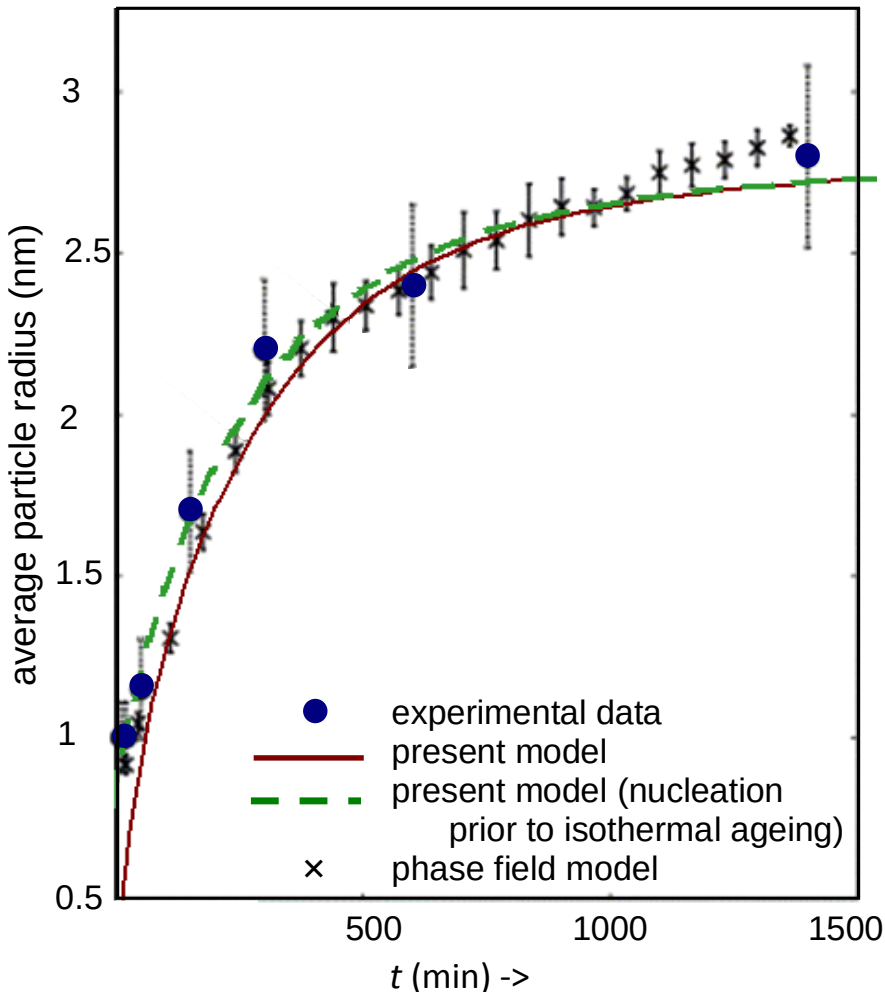

Fig 8. Mean particle size of Ni_3Al precipitates for Ni-14at%Al aged at 823K. The experimental results are taken from Wendt and Haasen [42]. Red lines are the present model with n=1½ and particle nucleating at t=0, the green dashed line is for the present model with n=1½ and particles present at the start of isothermal ageing. Simulated size evolution using a phase field model is taken from [32].

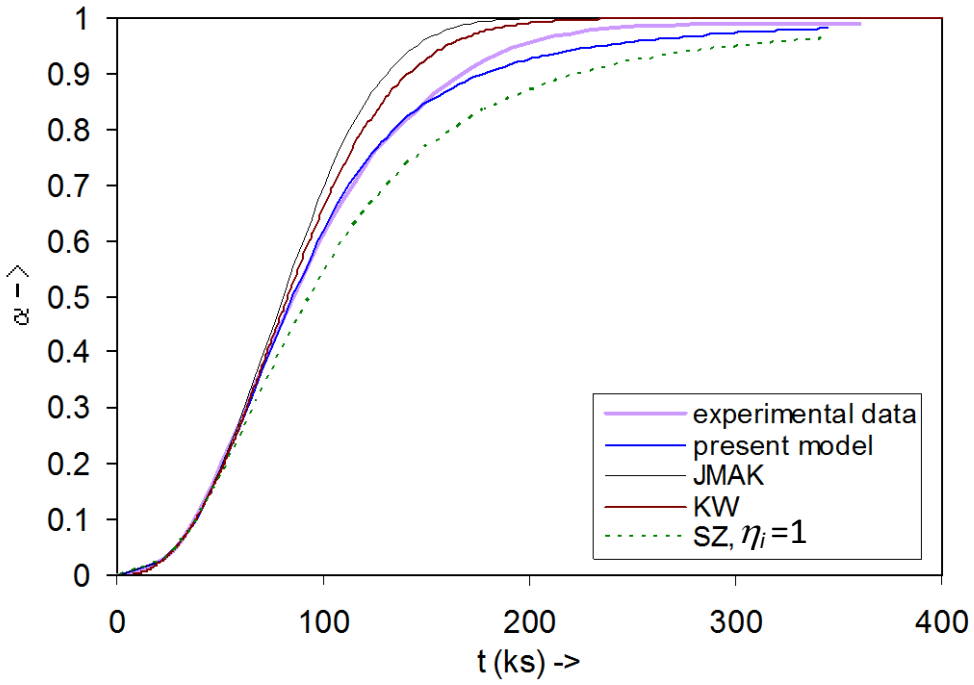

Fig 9. Fraction transformed vs ageing time at 403K for GP zone formation in an Al-5.8at%Zn alloy as obtained from microcalorimetry experiments. The experimental data is compared with 4 models: Kampmann Wagner (KW) for a dilute alloy, Starink-Zahra (SZ) for η_i=1, JMAK and the present new model (Eq. 7).

Figure Captions

Fig. 1. Schematic depiction of the depletion fraction (1- χ) as a function of the volume in the extended volume for a diffusion-controlled reaction a) approximation used if one was to use JMAK kinetics to approximate a diffusion-controlled reaction (a poor approximation), and b) linear $\chi - V$ approximation (the much improved approximation used to derive the present new model).

Fig. 2. Fraction transformed vs extended fraction transformed for 4 models: Kampmann Wagner (KW) for a dilute alloy, Starink-Zahra (SZ) for η_i=1, JMAK and the present new model (Eq. 8).

Fig. 3. Schematic illustration of impingement for 2 dimensional growth of a fixed number of nuclei. There are 4 nuclei in this section (yellow) with a partially depleted matrix around them. Each grey scale represents an interval of the depletion fraction, χ. Iso depletion contours are segments of circles.

Fig. 4. Fraction transformed for various precipitation reactions vs t/A, with t the isothermal ageing time and A for each reaction chosen such that $t(\alpha=0.5)$ coincides. Data from [Wea]=[59], [Boo]=[45], [Roy]=[41], [Deh]=[43], [Jo]=[42], [Yon]=[51].

Fig. 5. Fraction transformed vs the ageing time, t, for on Al_3Sc formation in Al-0.2 wt% Sc from Røyset and Ryum [41]. Black lines are model calculations reported by Fan et al. [32] using their model [32], colored lines are the present model with $n=2½$ (for the 2 higher temperatures) and $n=1½$ for the lower temperature.

Fig. 6. Amount of product phase vs the annealing time, t, in ferrite formation in isothermal annealing of 0.37C-1.45Mn-0.11V micro-alloyed steel with prior austenite grain size 76 μm. Specimens was austenitized at 1523 K for 1 min and then rapidly quenched to 973 K for isothermal annealing. Data from [30]. Experimental data is compared with 4 models with $k=0.011$, $n=0.5$. Main graph is on log time scale, inset on linear time scale. Typical error bar is shown for one point.

Fig. 7. The evolution of the precipitate volume fraction for Ni– 6.5 at% Al–9.5 at% Cr at 873 K (data from Booth-Morrison et al. [45]). The volume fraction in is fitted by the new model.

Fig. 8. Mean particle size of Ni_3Al precipitates for Ni-14at%Al aged at 823K. The experimental results are taken from Wendt and Haasen [44]. Red lines are the present model with $n=1½$ and particle nucleating at t=0, the green dashed line is for the present model with $n=1½$ and particles present at the start of isothermal ageing. Simulated size evolution using a phase field model is taken from [35].

Fig. 9. Fraction transformed vs ageing time at 403K for GP zone formation in an Al-5.8at%Zn alloy as obtained from microcalorimetry experiments. The experimental data is compared with 4 models: Kampmann Wagner (KW) for a dilute alloy, Starink-Zahra (SZ) for $\eta_i=1$, JMAK and the present new model (Eq. 8).

References

1 F. Liu, F. Sommer, C. Bos, E.J. Mittemeijer, Int. Mater. Rev. 52 (2007) 193–212.
2 M.J. Starink. Int Mater Rev, 2004, 49, 191-226.
3 D.H. Bratland, Ø. Grong, H. Shercliff, O.R. Myhr, S. Tjotta. Acta Mater 1997; 45, 1-22.
4 H. Wang, F. Liu, T. Zhang, G. Yang, Y. Zhou. Acta Mater 2009; 57, 3072-3083.
5 R. Kampmann, R. Wagner. in Decomposition of Alloys: the Early Stages, Haasen P, Gerold V, Wagner R, Ashby MF (Eds.), New York, Pergamon Press, 1984, 91-103.
6 O.R. Myhr, Ø. Grong. Acta Mater 2000; 48, 1605.
7 J.D. Robson, PB Prangnell. Acta Mater 2001; 49, 599-613.
8 J.D. Robson. Acta Mater 2004; 52, 1409-1421.
9 I.N. Khan, M.J. Starink, J.L. Yan. Mater Sci Eng A 2008; 472, 66-74

10 O.R. Myhr, Ø. Grong, A.J. Anderson. Acta Mater 2001;49:65-75
11 Miyazaki T, Koyama T, Kobayashi S. Metall Mater Trans A 1996;27,945–949.
12 Ø. Grong, O.R. Myhr. Acta Mater 2000; 48, 445-452.
13 P Bruna, D Crespo, R González-Cinca, E Pineda, J. Appl. Phys. 100 (2006) 054907.
14 M. Tomellini, Comp. Mater. Sci. 50 (2011) 2371–2379
15 J. Svoboda, E. Gamsjàger, F.D. Fischer, P. Fratzl. Acta Mater 52 (2004) 959–967
16 E. Kozeschnik, J. Svoboda, P. Fratzl , F.D. Fischer, Mater Sci Eng A, 385, 2004, 157 - 165.
17 L. Onsager, Phys. Rev. I 37 (1931) 405.
18 F.L. Cumbrera, F. Sánchez-Bajo, Thermochim Acta 1995, 266, 315-330.
19 M. Avrami. J Chem Phys 1940; 8, 212.
20 M.J. Starink. J Mater Sci 1997; 32, 4061.
21 A.N. Kolmogorov. Izv Akad Nauk SSSR Ser Mater 1937; 1, 355.
22 A.A. Burbelko, E. Fraś, W. Kapturkiewicz. Mater Sci Eng A 2005; 413–414, 429-434.
23 M. Tomellini, Thermochim Acta 2013, 566, 249-256.
24 W.A. Johnson, K.E. Mehl, Trans Am Inst Min Met Engrs 1939; 195, 416
25 M. Avrami. J Chem Phys 1941; 9, 177.
26 M.J. Starink. J Mater Sci, 2001, 36, 4433-4441.
27 M.J. Starink, A-M Zahra. Thermochim Acta, 1997, 292, 159-168.
28 F. Liu, S.J. Song, F. Sommer, E.J. Mittemeijer. Acta Mater 57, 2009; 6176-6190.
29 J.B. Austin, R.L. Rickett. Trans Am Inst Min Engrs 1939; 135, 396.
30 C. García de Andreś, C. Capdevila, F.G. Caballero, H.K.D.H. Bhadeshia. Scr Mater 1998; 39, 853–859.
31 S.E. Offerman, N.H. van Dijk, J. Sietsma, E.M. Lauridsen, L. Margulies, S. Grigull et al. Acta Mater 2004; 52, 4757-4766.
32 K. Fan, F. Liu, X.N. Liu, X.Y. Zhang, G.C. Yang, Y.H. Zhou. Acta Mater 2008; 56, 4309-4318.
33 R. Mukherjee, T.A. Abinandanan, M.P. Gururajan. Acta Mater 2009; 57, 3947-3954.
34 P. Bruna, E. Pineda, J.I. Rojas, D. Crespo, J All Comp 483, 2009, 645.
35 Y.H. Wen, B. Wang, J.P. Simmons, Y. Wang. Acta Mater 2006; 54, 2087-2099.
36 F.S. Ham. Phys. Chem. Solids. 6, 1958, 335-351.
37 C. Shen. PhD thesis, Ohio State University, 2004.
38 S.J. Song, F. Liu, Y.H. Jiang. J Mater Sci 2012; 47, 5987-5995.
39 C. Capdevila, F.G. Caballero, C. Garcıa de Andres. Metall Mater Trans A 2001; 32:661
40 M.J. Starink. in preparation, 2014
41 J. Røyset, N. Ryum. Mater Sci Eng A 2005; 396, 409-422.
42 Hyung-Ho Jo, S.I. Fujikawa. Mater Sci Eng A 1993; 171, 151
43 M. Dehmas, A. Maitre, J.B. Richir, P. Archambault. J Power Sources 2006 ; 159, 721-727.
44 H. Wendt, P. Haasen. Acta Metall 1983; 31, 1649.
45 C. Booth-Morrison, Y. Zhou, R.D. Noebe, D.N. Seidman. Philosoph Mag 2010; 90, 219–235.
46 S.Q. Xiao, P. Haasen. Acta Metall Mater 1991; 39, 651-659.
47 J.B. Gilmour, G.R. Purdy, J.S. Kirkaldy. Metall Trans 1972; 3, 3213.
48 C. Capdevila, F.G. Caballero, C. Garcia de Andres. Scripta Mater 2001; 44, 593-600.
49 M. Tong, D. Li, Y. Li, J. Ni. Metall Mater Trans A 2002; 33, 3111-3115.
50 J. Sietsma, S. van der Zwaag. Acta Mater 2004; 52, 4143–4152.
51 Y. Liu, D. Wang, F. Sommer, E.J. Mittemeijer. Acta Mater 2008; 56, 1359-6454.
52 C.R. Hutchinson, A. Fuchsmann, Y. Brechet. Metall Mater Trans A 2004; 35: 1211–1221.
53 R. Badji, M. Bouabdallah, B. Bacroix, C. Kahloun, K. Bettahar, N. Kherrouba. Mater Sci Eng A 2008; 496, 447-454.
54 Y. Sutou, N. Koeda, T. Omori, R. Kainuma, K. Ishida. Acta Mater 2009; 57, 5748-5758.
55 L.C. Chang. Mater Sci Eng A 2004; 368, 175-182.

56 D. Quidort, Y.J.M. Brechet. Acta Mater 2001 ; 49, 4161-4170.
57 S. Bartels, W. Gruber, B. Cappi, R. Telle, H. Schmidt. Mater Lett 2008; 62, 3836-3838.
58 P. Huang, R.F. Hochman. Mater Sci Eng A 1989; 115, 257-260.
59 C.W. Weaver. Acta Metall 1962; 10, 1151-1160.
60 R.C. Tucker Jr., T.E. Scott, O.N. Carlson. J Less Common Metals 1971; 24, 405-418.
61 M.J. Starink, A.-M. Zahra. Phil Mag A 1997; 76, 701-714.
62 M.J. Starink, A.-M. Zahra. Phil Mag A 1998; 77, 187-199.
63 M. Nishi, T. Kubo, T. Kato, A. Tominaga, K. Funakoshi, Y. Higo. Phys Earth Planet Interiors 2011; 189, 47–55
64 Haipeng Wang, A. Pring, Y. Ngothai, B. O'Neill. Geochim Cosmochim Acta 2005; 69, 415-425.
65 M.J. Starink, S.C. Wang. Acta Mater 2009; 57, 2376-2389
66 M.J. Starink. J Mater Sci Lett 1996; 15, 1749.
67 K. Fan, F. Liu, K. Zhang, G.C. Yang, Y.H. Zhou. J Crystal Growth 2009; 311, 4660–4664.
68 M.J Starink, P. van Mourik, Mater. Sci. Eng. A 156, 1992, 183-194
69 P. van Mourik, T.H. de Keijser, E.J. Mittemeijer, Scr metall 1987, 21, 381-385
70 I. Gutierrez-Urrutia, J. Mater. Sci., 46, 2011, 3144-3150
71 S.I. Vooijs, S.B. Davenport, I. Todd, S. van der Zwaag, Phil. Mag. 81, 2001, 2059-2072
72 C. Capdevila, M.K. Miller, J. Chao, Acta Mater., 60, 2012, 4673-4684,
73 M.J Starink, A.-M. Zahra, Thermochim. Acta 298, 1997, 179-189